ChemPhysChem

Research Article
doi.org/10.1002/cphc.202300165

Chemistry Europe
European Chemical Societies Publishing

www.chemphyschem.org

Quantum Chemical Study of the Pressure-dependent Phosphorescence of $[Cr(ddpd)_2]^{3+}$ in the Solid State

Christoph Förster,[a] Helena Osthues,[b] Dominik Schwab,[b] Nikos L. Doltsinis,*[b] and Katja Heinze*[a]

The chromium(III) complex $[Cr(ddpd)_2][BF_4]_3$ shows two spin-flip emission bands in the near-infrared spectral region. These bands shift bathochromically by −14.1 and −7.7 $cm^{-1}kbar^{-1}$ under hydrostatic pressure (*Angew. Chem. Int. Ed.* **2018**, *57*, 11069). The present study elucidates the structural changes of the chromium(III) cations under pressure using density functional theory with periodic boundary conditions and the resulting effects on the excited state energies using high-level CASSCF-NEVPT2 calculations. The differences of the bands in pressure sensitivity are traced back to a different orbital occupation of the intraconfigurational excited states.

Introduction

Luminescent materials have found numerous applications, for example in light-emitting devices,[1] circularly polarized emission,[2] lasing,[3] optical data storage,[4] quantum computing,[5] energy conversion schemes[6] and sensing.[7] Typically, precious metal ions or lanthanide ions provide the required luminescence properties, but complexes of earth-abundant transition metal ions have recently been developed to successfully enter several of these fields.[8] In particular, novel copper(I), molybdenum(0) and chromium(III) complexes possess properties approaching or even surpassing those of the precious metal ions or lanthanide ions.[8]

For pressure sensing, the R_1 line ($^2E \rightarrow {}^4A_2$ spin-flip transition, notation for octahedral symmetry) of ruby $Al_2O_3:Cr^{3+}$ is most commonly used,[9] for example in diamond anvil cells, yet other materials with larger sensitivity have been developed, for example based on lanthanide ions exploiting their sharp emission bands.[10]

All these optical pressure sensors are typically solid state materials such as oxides or halide lattices of lanthanide or chromium ions. Luminescent chromium(III)-based materials show small pressure-induced shifts of the chromium(III) R_1 line between −0.6 to −3.77 $cm^{-1}kbar^{-1}$ (Table 1).[9,11,12] Classical chromium(III) complexes with oxalato (ox^{2-}), ammine, urea or fluorido ligands exhibit moderate pressure-induced shifts of −2.5 to −7.8 $cm^{-1}kbar^{-1}$ besides their rather poor luminescence quantum yields (Table 1).[13–16]

With the development of the highly emissive molecular polypyridine chromium(III) complex $[Cr(ddpd)_2]^{3+}$[17] and its congeners (molecular rubies),[18–20,2b] very large pressure-induced shifts $\Delta\tilde{\nu}_2/\Delta p$ of −13.0 to −14.1 $cm^{-1}kbar^{-1}$ have been achieved in the solid state (Table 1; energy E_2).[7b] Spin-flip emitters with other metal ions or d electron configurations[21] can show different behavior, which might also depend on the ground state splitting.[22] As the $^4A_2$ ground state of chromium(IIII) ions is orbitally non-degenerate, the ground state splitting plays no role here (Figure 1).

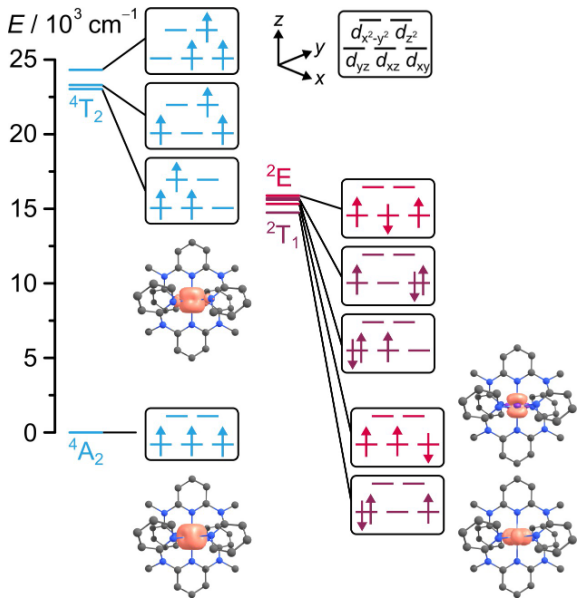

Figure 1. Computationally derived state diagram at the ground state geometry of $[Cr(ddpd)_2]^{3+}$ with dominating electron configurations in the microstates and calculated spin-densities at an isosurface value of 0.05 a.u. of states relevant to this study.[7b,8c]

[a] *Dr. C. Förster, Prof. Dr. K. Heinze*
Department of Chemistry
Johannes Gutenberg University Mainz
Duesbergweg 10–14, 55128 Mainz, Germany
E-mail: katja.heinze@uni-mainz.de
[b] *H. Osthues, D. Schwab, Prof. Dr. N. L. Doltsinis*
Institut für Festkörpertheorie and Center for Multiscale Theory and Computation
Westfälische Wilhelms-Universität Münster
Wilhelm-Klemm-Str. 10, 48149 Münster, Germany
E-mail: nikos.doltsinis@wwu.de

Supporting information for this article is available on the WWW under https://doi.org/10.1002/cphc.202300165

Table 1. Energies (E_1 and E_2) at ambient pressure and pressure-induced shifts ($\Delta\tilde{\nu}_1/\Delta p$ and $\Delta\tilde{\nu}_2/\Delta p$) of the spin-flip emission bands of selected chromium(III) materials.

	E_1 [cm^{-1}]	E_2 [cm^{-1}]	$\Delta\tilde{\nu}_1/\Delta p$ [$cm^{-1}\,kbar^{-1}$]	$\Delta\tilde{\nu}_2/\Delta p$ [$cm^{-1}\,kbar^{-1}$]	ref.
$BeAl_2O_4:Cr^{3+}$	14699		−0.6		[11]
$Al_2O_3:Cr^{3+}$	14405		−0.7		[9]
$Cs_2NaYCl_6:Cr^{3+}$	14415		−3.77		[12]
$Na[Ru(bpy)_3][Cr(ox)_3]$	14387-14418		−2.5		[13]
$[Cr(NH_3)_6][NO_3]_3$	15224		−4		[14]
$[Cr(urea)_6][ClO_4]_3$	14191		−5.5		[15]
$[NH_4]_3[CrF_6]$	15583		−7.8		[16]
$[Cr(H_2tpda)_2][ClO_4]_3$	13503	12743	−8.4	−13.0	[7b]
$[Cr(ddpd)_2][PF_6]_3$	13511	12827	−4.7	−13.0	[7b]
$[Cr(ddpd)_2][BF_4]_3$	13492	12811	−7.7	−14.1	[7b]
$[Cr(ddpd)_2][BF_4]_3/H_2O$	13556	12876	−9.5	−14.8	[7b]
$[Cr(ddpd)_2][BF_4]_3$/MeOH	13554	12872	−9.8	−14.5	[7b]

Even the weaker emission from the next higher energy level (energy E_1 in Table 1) which is in equilibrium with the lowest energy level[7c,8c] (energy E_2 in Table 1) can be observed with good signal-to-noise ratio. From high-level CASSCF-NEVPT2 calculations the lowest emissive state (energy E_2) derives from a spin-paired spin-flip state of $^2T_1$ origin, while the higher emissive state (energy E_1) derives from a true spin-flip state of ^2E origin (Figure 1).[7b,8c] In contrast, the lowest emissive state is reported as a ^2E state for the classical chromium(III) complexes such as $[Cr(ox)_3]^{3-}$, $[Cr(NH_3)_6]^{3+}$, $[Cr(urea)_6]^{3+}$ and $[CrF_6]^{3-}$.[13–16]

The exceptionally large quantum yields and solubility of the molecular rubies in water or methanol allowed the detection of pressure-induced shifts for both emission bands even in solution (Table 1).[7b] When changing the counter ions or the environment (crystal/solution), the more pronounced shift of the $^2T_1 \rightarrow {}^4A_2$ (E_2) emission band of $[Cr(ddpd)_2]^{3+}$ varies merely between −13.0 and −14.8 $cm^{-1}\,kbar^{-1}$, while the shift of the higher-energy band $^2E \rightarrow {}^4A_2$ (E_1) is more affected with a variation from −4.7 to −9.8 $cm^{-1}\,kbar^{-1}$.[7b] Consequently, the energy gap between the two lowest emissive doublet states of ^2E and $^2T_1$ character increases with increasing pressure, but to a different extent in varying environments. Notably, the smaller ^2E emission shift of $[Cr(ddpd)_2]^{3+}$ is relatively close to the ^2E shift range of the classical chromium(III) complexes (Table 1). Ligand field calculations had suggested that the most decisive parameters influencing the emission energies under hydrostatic pressure are geometrical distortions of the $[Cr(ddpd)_2]^{3+}$ cation, while mere changes of the ligand field splitting, the Racah parameters *B* and *C* or spin-orbit coupling (SOC) do not explain the observed spin-flip emission band shifts.[7b]

However, the nature of the distortions leading to the observed large energy shifts of the $^2E/^2T_1 \rightarrow {}^4A_2$ emission bands as well as the effect of the environment (counterions, solvents) on the energies of the two spin-flip bands are not well understood. The present study aims to clarify the nature of the distortions of the $[Cr(ddpd)_2]^{3+}$ cation under pressure and the resulting distinct effects on the luminescence bands using a computational approach combining density functional theory (DFT) with periodic boundary conditions for the geometries at different pressure and high-level CASSCF-NEVPT2 calculations on the optimized geometries under pressure for the relevant excited state energies. Finally, we suggest an answer to the question why the polypyridine chromium(III) complexes display significantly larger pressure-induced shifts than previously reported chromium(III) complexes (Table 1).

Results and Discussion

Pressure Effects on the Geometry in the Solid State

$[Cr(ddpd)_2][BF_4]_3 \times 3CH_3CN$ (CCDC access code 1059802) crystallizes in the monoclinic space group *P*n with *a*, *b*, *c* = 11.5125(8), 16.5554(11), 12.9721(9) Å, β = 111.890(2)° and V = 2294.2(3) Å^3 at 173 K.[17a] The asymmetric unit contains a $[Cr(ddpd)_2]^{3+}$ trication, three tetrafluoroborate counter ions (with two of them being orientationally disordered) and three acetonitrile solvate molecules.

The entire unit cell and the geometry were optimized using DFT with periodic boundary conditions without symmetry constraints (Figure 2, see Computational Details) for different external isotropic pressures of 1.0, 28, 56 and 84 kbar. The lower symmetry employed in the calculations leads to two independent chromium(III) complexes (Cr/Cr′), which will both be considered. While the pressure-induced changes to the cell angles are relatively minor, suggesting that the monoclinic crystal system is essentially preserved, the lattice constants *a*, *b*, and *c* are more strongly affected (Table 2). Increasing the pressure from 1.0 kbar to 28 kbar causes *a*, *b*, and *c* to shrink by 4.0%, 5.6% and 6.0%, respectively, corresponding to a rather isotropic compression. The unit cell volume *V* decreases by 15% at 28 kbar and by 25% at 84 kbar relative to 1 kbar (Table 2).

From the unit cell volumes calculated at 1 and 84 kbar, the bulk modulus $K = -V\,dp/dV$ of $[Cr(ddpd)_2][BF_4]_3 \times 3CH_3CN$ is estimated as $K([Cr(ddpd)_2][BF_4]_3) = 331$ kbar. This is eight times smaller than that of ruby $Al_2O_3:Cr^{3+}$ [$K(Al_2O_3:Cr^{3+}) = 2530$ kbar],[23] but closer to the more compressible chloride lattice of $Cs_2NaYCl_6:Cr^{3+}$ [$K(Cs_2NaYCl_6:Cr^{3+}) \approx 495$ kbar].[12] A smaller bulk modulus correlates with a larger pressure-induced shift of the emission bands $\Delta\tilde{\nu}/\Delta p = -7.7/-14.1$,

Research Article
doi.org/10.1002/cphc.202300165

Chemistry Europe
European Chemical Societies Publishing

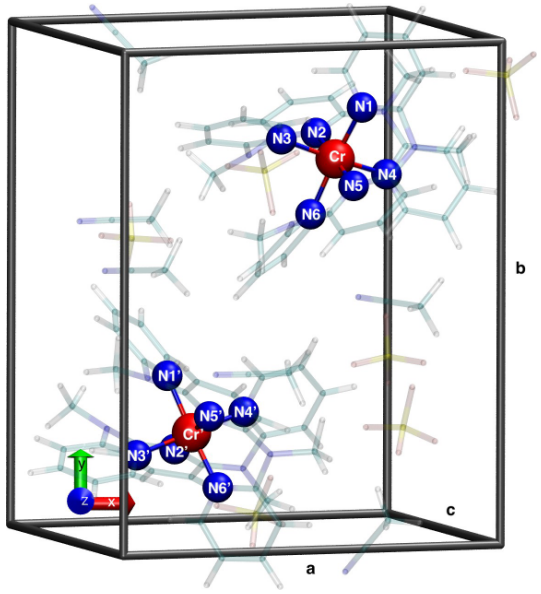

Figure 2. Optimized unit cell of $[Cr(ddpd)_2][BF_4]_3 \times 3CH_3CN$ at 1 kbar. The atom labels correspond to the notation used in Tables 2 and 3 (red = Cr, blue = N, yellow = B, pink = F, turquoise = C, white = H).

−3.77 and −0.7 $cm^{-1}kbar^{-1}$ for $[Cr(ddpd)_2][BF_4]_3$, Cs_2NaYCl_6:Cr^{3+} and Al_2O_3:Cr^{3+}, respectively (Table 1).[7b,12,9]

At 1 kbar, the chromium(III) complex cation denoted by Cr shows close contacts to two $[BF_4]^-$ counter ions with Cr···F distances of 5.39 and 6.51 Å. Additionally, a CH_3CN molecule has a short contact to the chromium(III) center of Cr···N(CH_3CN) = 4.63 Å. At 84 kbar, these Cr···F and Cr···N(CH_3CN) distances shrink to 4.42, 5.80 and 4.38 Å, respectively (Cr complex in Figure 2). Similarly, the respective Cr′···F′ and Cr′···N′ distances of the other cation denoted Cr′ shorten from 6.28, 7.08 and 4.71 Å to 5.45, 6.69 and 4.16 Å, respectively. The Cr–N distances to the polypyridine ligand shorten from 2.045 to 2.000 Å (−2.2%) on average from 1 to 84 kbar, (Table 3, Cr). The N–Cr–N angles are affected with small changes from 0.02 to 3.29° (max. 3%) upon pressure increase from 1 to 84 kbar (Table 4, Cr). Consequently, the Cr–N bond length shrinkage affects both σ and π bonding, while the octahedricity of the CrN_6 polyhedron is not strongly affected by the pressure increase. The structure of the Cr′ cation experiences similar pressure effects (Cr′ complex in Figure 2, Tables 2, 3).

The torsional angles between trans-coordinated pyridines amount to −94.7, 73.1 and 17.2° and −82.5, 72.9 and 12.2° (Cr) [−75.2, 71.2 and −14.4° and −101.9, 71.9 and −4.6° (Cr′)] for the four terminal and the two central pyridines at 1 and

Table 2. Optimized cell parameters of $[Cr(ddpd)_2][BF_4]_3 \times 3CH_3CN$ and relative energies for different external pressures.

p [kbar]	*V* [Å^3]	*a* [Å]	*b* [Å]	*c* [Å]	*α* [°]	*β* [°]	*γ* [°]	*E* [eV]
1.0	2258.04	11.38	16.48	13.02	90.31	112.35	90.41	0.00
28.0	1927.54	10.93	15.56	12.24	89.94	112.14	90.11	2.37
56.0	1792.83	10.62	15.16	12.06	90.19	112.60	90.10	5.92
84.0	1692.40	10.53	14.92	11.60	89.81	111.87	90.31	9.88

Table 3. Cr–N bond lengths (in Å) for different pressures of the two complex cations Cr / Cr′.

bond	1 kbar	28 kbar	56 kbar	84 kbar
Cr–N1	2.040/2.044	2.023/2.026	2.000/2.014	1.987/2.002
Cr–N2	2.043/2.042	2.031/2.032	2.027/2.020	2.016/2.010
Cr–N3	2.041/2.038	2.020/2.020	2.001/2.009	1.988/1.992
Cr–N4	2.054/2.052	2.038/2.039	2.017/2.016	2.003/2.004
Cr–N5	2.048/2.049	2.032/2.034	2.022/2.022	2.007/2.008
Cr–N6	2.044/2.041	2.027/2.023	2.015/2.016	2.004/1.992

Table 4. N–Cr–N bond angles (in degrees) for different pressures of the two complex cations Cr/Cr′.

angle	1 kbar	28 kbar	56 kbar	84 kbar
N1–Cr–N2	94.94/94.70	94.41/94.41	93.41/94.64	92.91/95.44
N1–Cr–N3	89.64/90.18	90.18/90.30	90.53/90.02	90.88/89.98
N1–Cr–N4	91.16/89.84	91.03/90.05	90.24/89.93	90.20/90.80
N1–Cr–N5	86.03/85.38	86.11/85.06	86.03/84.73	86.37/84.75
N2–Cr–N3	85.33/85.57	84.99/84.90	84.89/84.48	84.99/84.72
N2–Cr–N4	85.53/85.21	83.98/83.90	83.53/83.05	83.06/82.73
N2–Cr–N6	93.58/93.92	94.31/94.43	95.58/94.90	95.81/93.06
N3–Cr–N5	94.40/94.79	94.73/94.88	94.83/96.45	95.48/96.09
N3–Cr–N6	91.01/89.55	90.43/90.35	90.35/91.66	89.87/90.99
N4–Cr–N5	94.74/94.43	96.30/96.31	96.75/96.01	96.47/96.47
N4–Cr–N6	89.55/91.81	90.03/91.03	90.68/90.48	90.86/90.09
N5–Cr–N6	85.46/86.01	85.17/86.10	84.98/85.73	84.91/86.74
N1–Cr–N6	171.49/171.33	171.28/171.16	171.01/170.43	171.28/171.49
N2–Cr–N5	178.99/179.63	179.41/179.43	179.37/178.86	179.14/179.17
N3–Cr–N4	170.87/170.75	168.97/168.79	168.42/167.49	168.04/167.44

84 kbar, respectively. Clearly, the terminal pyridines are oriented almost orthogonal to each other, while the central pyridines are more coplanar. One pair of terminal trans-coordinated pyridines does not twist at all under pressure, while the other terminal pyridine pair undergoes a small torsional motion around the orthogonal orientation from +4.3 to −7.5° (Cr) and from +11.9 to −14.8° (Cr′) at 1 and 84 kbar, respectively. The pair of central pyridines becomes more coplanar at 84 kbar in both cations.

In summary, the structure analysis suggests a small compression of the Cr–N bonds (2.2%) and a co-planarization of the central pyridines of the ddpd ligands as major geometric effects upon pressurizing from 1 to 84 kbar. This will affect both the Cr–N σ and π bonding, respectively.

Pressure Effects on the Electronic Structure of the Excited States

The optimized geometries of the trications (Cr and Cr′) at pressures of 1, 28, 56 and 84 kbar were used as input coordinates for CASSCF(13,10)-NEVPT2 calculations (see Computational Details).[7b,17a,18,22,24–26] The active space comprises the five 3d orbitals, two occupied Cr–N σ-bonding and three occupied π-bonding orbitals. The derived energy levels of the lowest excited quartet and doublet states of Cr are depicted in Figure 3. The corresponding data for Cr′ can be found in the Supporting Information (Figures S1–S5, Tables S1 and S2).

As expected, the interconfigurational $^4T_2$ derived levels linearly increase strongly in energy with increasing pressure ($\Delta\tilde{\nu}_{3,calcd}/\Delta p = +(20.6-32.3)\ cm^{-1}\,kbar^{-1}$) as a result of a compressed coordination polyhedron increasing the ligand field splitting and the population of Cr–N σ-antibonding orbitals in the $^4T_2$ derived states (Figure 3, Supporting Information Table S2). The energy of the $^4T_2(2)$ microstate, corresponding to a $d_{xy}\rightarrow d_{x2-y2}$ transition, shows the highest pressure sensitivity within the $^4T_2$ state manifold (Figure 3, Supporting Information Figure S1, Tables S1 and S2). Figure 4a depicts the relevant antibonding singly occupied d_{x2-y2} orbital. The pressure sensitivity coincides with the slightly stronger Cr–N bond compression involving Cr and the peripheral pyridine donors N1/N3/N4/N6 of 0.049 Å (average, Cr), compared to Cr and the central pyridine donors N2/N5 with 0.034 Å (average, Cr, Table 3). The energies of the doublet levels derived from ^2E and $^2T_1$ terms drop linearly in energy with increasing pressure (Figure 3, Supporting Information Figure S1). The calculated shift of the lower energy $^2T_1$ derived state ($\Delta\tilde{\nu}_{2,calcd}/\Delta p = -6.9\ cm^{-1}\,kbar^{-1}$) is roughly twice as large compared to the next higher ^2E derived state ($\Delta\tilde{\nu}_{1,calcd}/\Delta p = -3.1\ cm^{-1}\,kbar^{-1}$). For the Cr′ cation similar values of $\Delta\tilde{\nu}_{2,calcd}/\Delta p = -6.5\ cm^{-1}\,kbar^{-1}$ and $\Delta\tilde{\nu}_{1,calcd}/\Delta p = -3.3\ cm^{-1}\,kbar^{-1}$ are calculated. These shifts match the trend of the experimental shifts of $\Delta\tilde{\nu}_{2,exp}/\Delta p = -14.1\ cm^{-1}\,kbar^{-1}$ and ($\Delta\tilde{\nu}_{1,exp}/\Delta p = -7.7\ cm^{-1}\,kbar^{-1}$. Importantly, the combined DFT/CASSCF calculations correctly reproduce the larger shift of the lower energy band by a factor of two ($f_{exp} = 1.8$; $f_{calcd} = 1.9$–2.0).

This higher sensitivity of the lowest energy $^2T_1$ derived state seems to be associated with the paired electron spins in the t_{2g} shell, a combination of the d_{xz}/d_{yz} orbital (Figure 4b) possessing π symmetry with respect to the central pyridines. This π interaction increases with the co-planarization of the central pyridines at higher pressure possibly allowing for a stronger delocalization of the d electrons onto the central pyridines and hence increasing the nephelauxetic effect. On the other hand, the lowest true ^2E-derived spin-flip state lacks electron pairs in the t_{2g} shell (Figure 1).

The exceedingly strong pressure sensitivity of the low-energy luminescence band of the molecular ruby $[Cr(ddpd)_2]^{3+}$ is a consequence of the excited state inversion, so that the low-energy band corresponds to emission from an essentially $^2T_1$-derived microstate with paired electrons in a t_{2g} orbital instead

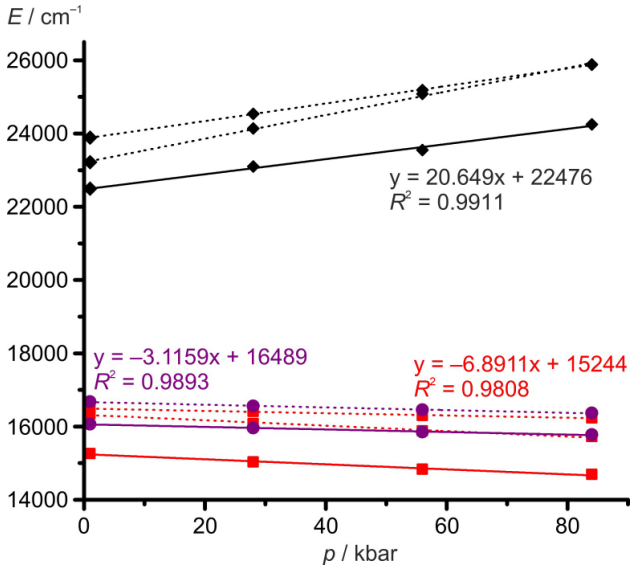

Figure 3. Energies of the $^4T_2$ (black), ^2E (purple) and $^2T_1$ (red) terms of the Cr cation. All levels which are doubly or triply degenerate in octahedral symmetry are split (see also Figure 1). Solid lines are linear fits to the CASSCF-calculated energy values of the lowest energy microstates of a given term. Dotted lines represent the higher energy microstates. The respective slopes are given for the lowest energy $^4T_2$, ^2E and $^2T_1$ microstates $^4T_2(1)$, $^2E(1)$ and $^2T_1(1)$.

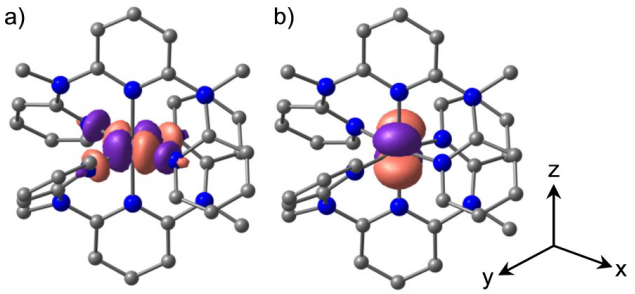

Figure 4. Canonical orbitals relevant for a) the $^4T_2(2)$ state (d_{x2-y2}, singly occupied) and b) the lowest energy $^2T_1(1)$ state (d_{xz}/d_{yz} combination, doubly occupied) depicted at a contour value of 0.05 a.u. Hydrogen atoms omitted for clarity. Molecular coordinate system indicated.

of the emission from ^{2}E-derived states of classical chromium(III) complexes.[13–16]

Conclusion

The pressure-dependencies of the two emission bands of a molecular ruby $[Cr(ddpd)_2]^{3+}$ has been modelled using a combination of DFT with periodic boundary conditions for the geometries at different pressures and high-level CASSCF-NEVPT2 calculations on the respective optimized geometries for the relevant excited state energies. The largest structural changes upon pressurizing from 1 to 84 kbar are the Cr–N bond compressions by 2.2% and the co-planarization of the central pyridines of the tridentate ddpd ligands.

The interconfigurational $^4T_2$-derived levels increase in energy due to the population of d_σ $(e_g^*)^1$ orbitals and the pressure-induced compression of the Cr–N bonds. The lowest $^4T_2$ derived microstate experiences a strong pressure shift with $\Delta\tilde{\nu}_{,calcd}/\Delta p = +21.0 \pm 0.4\ cm^{-1}\,kbar^{-1}$. The intraconfigurational states derived from $^2T_1$ and ^{2}E terms, respectively, shift to lower energy under pressure. While the shift of the lowest ^{2}E-derived state is in the range of typical shifts of classical chromium(III) emitters ($\Delta\tilde{\nu}_{1,calcd}/\Delta p = -3.2 \pm 0.3\ cm^{-1}\,kbar^{-1}$) with this state being the lowest energy excited state, the shift of the lowest $^2T_1$-derived state is roughly twice as large ($\Delta\tilde{\nu}_{2,calcd}/\Delta p = -6.7 \pm 0.3\ cm^{-1}\,kbar^{-1}$). The doubling of the shift is also found experimentally. This difference in pressure sensitivity is traced back to the double occupation of a d_π orbital of the t_{2g} set, which profits from a stronger π interaction with the pyridine ligands under pressure. A quantitative quantum chemical prediction of these small pressure-induced shifts is not yet achieved which might be associated with finding the global minimum structure under pressure by DFT, anharmonicities of the involved molecular vibrations or distortions of the excited states which might be more relevant for the $^4T_2$ derived states than the spin-flip states.

If the above given interpretation is valid in general, the pressure dependence of spin-flip emission bands might help to experimentally differentiate the spin-paired spin-flip state from the true spin-flip state. Experimental and theoretical studies on other d^3 and d^2[22] emitters under pressure will be performed in the future to test this hypothesis.

Computational Details

The DFT calculations were performed using the CP2k software package[27] with a combination of triple zeta basis with one polarization function (TZVP) Gaussian basis[28] and plane waves with a 600 Ry kinetic energy cutoff together with Goedecker-Teter-Hutter pseudopotentials.[29–31] The PBE density functional[32] with Grimme's D3(BJ) dispersion corrections[33] was employed. No spin restriction is applied and the initial atomic guess of the singlet wave function is manipulated, such that the spin symmetry is broken. It was verified that other spin multiplicities yield higher energies than the singlet state. The Brillouin zone was sampled at the Γ k-point. Geometries were optimized until the forces were smaller than 4.5×10^{-4} a.u. The stress tensor was calculated analytically.[34] Initial unit cell parameters and geometries were taken from the experimental crystal structure determination (CCDC access code 1059802).[17a] The pressure was converged to within 0.1 kbar. No symmetry restrictions were applied.

The initial DFT and subsequent CASSCF calculations were performed using the quantum computing suite ORCA 5.0.3.[35,36] The initial active space was obtained from quasi-restricted DFT calculations using unrestricted Kohn-Sham orbitals DFT (UKS) and the B3LYP functional[37–39] in combination with Ahlrich's split valence triple-zeta basis set def2-TZVPP,[40] with the auxiliary basis def2/JK.[41] All DFT calculations make use of the resolution of identity (Split-RI-J) approach for the Coulomb term in combination with the chain-of-spheres approximation for the exchange term (keyword RIJCOSX).[42,43] The CASSCF calculations were performed with Ahlrich's split valence triple-zeta basis set def2-TZVPP,[40] with the auxiliary basis def2/JK.[41] All CASSCF calculations make use of the resolution of identity (Split-RI-JK) approach for the Coulomb and exchange term (keyword RIJK).[42,44] The calculations were performed state averaged with ten quartet and doublet roots, respectively. From CASSCF(3,5) results, the bonding counterparts to the metal centred orbitals were constructed (keyword IntOrbs PMOs). The final CASSCF(13,10) calculations were performed in conjunction with the strongly contracted N-electron valence perturbation theory to second order (SC-NEVPT2) in order to recover the missing dynamic correlation.[45,46] The zeroth order regular approximation was used in all calculations to describe relativistic effects in all calculations (keyword ZORA).[47–52] To account for environmental effects, a conductor-like screening model (keyword CPCM(acetonitrile)) modelling acetonitrile was used in all calculations.[53,54]

Acknowledgements

Parts of this research were conducted using the supercomputer Elwetritsch and advisory services offered by the Rheinland-Pfälzische Technische Universität Kaiserslautern-Landau (https://hpc.rz.rptu.de), which is a member of the AHRP and the Gauss Alliance e.V. This work was partially funded by the German Research Foundation within CRC 1459. Open Access funding enabled and organized by Projekt DEAL.

Conflict of Interest

The authors declare no conflict of interest.

Data Availability Statement

The data that support the findings of this study are available in the supplementary material of this article.

Keywords: chromium · luminescence · pressure · quantum chemical calculations · spin-flip

[1] a) C. Adachi, M. A. Baldo, S. R. Forrest, M. E. Thompson, *Appl. Phys. Lett.* **2000**, *77*, 904–906; b) C. Bizzarri, E. Spuling, D. M. Knoll, C. Volz, S. Bräse, *Coord. Chem. Rev.* **2018**, *373*, 49–82; c) R. D. Costa, E. Ortí, H. J. Bolink, F.

Monti, G. Accorsi, N. Armaroli, *Angew. Chem. Int. Ed.* **2012**, *51*, 8178–8211.
[2] a) B. Doistau, J. R. Jiménez, C. Piguet, *Front. Chem.* **2020**, *8*, 555; b) J.-R. Jiménez, B. Doistau, C. M. Cruz, C. Besnard, J. M. Cuerva, A. G. Campaña, C. Piguet, *J. Am. Chem. Soc.* **2019**, *141*, 13244–13252; c) C. Dee, F. Zinna, W. R. Kitzmann, G. Pescitelli, K. Heinze, L. Di Bari, M. Seitz, *Chem. Commun.* **2019**, *55*, 13078–13081; d) M. Deng, N. F. M. Mukthar, N. D. Schley, G. Ung, *Angew. Chem. Int. Ed.* **2020**, *59*, 1228–1231; e) J.-R. Jiménez, M. Poncet, S. Míguez-Lago, S. Grass, J. Lacour, C. Besnard, J. M. Cuerva, A. G. Campaña, C. Piguet, *Angew. Chem. Int. Ed.* **2021**, *60*, 10095–10102; *Angew. Chem.* **2021**, *133*, 10183–10190; f) E. E. Braker, N. F. M. Mukthar, N. D. Schley, G. Ung, *ChemPhotoChem* **2021**, *5*, 902–905.
[3] a) T. H. Maiman, *Nature* **1960**, *187*, 493–494; b) Z. S. Ngara, D. Okada, O. Oki, Y. Yamamoto, *Chem. Asian J.* **2019**, *14*, 1637–1641.
[4] V. W.-W. Yam, A. K.-W. Chan, E. Y.-H. Hong, *Nat. Chem. Rev.* **2020**, *4*, 528–541.
[5] a) D. W. Laorenza, D. E. Freedman, *J. Am. Chem. Soc.* **2022**, *144*, 21810–21825; b) D. Serrano, S. K. Kuppusamy, B. Heinrich, O. Fuhr, D. Hunger, M. Ruben, P. Goldner, *Nature* **2022**, *603*, 241–246, DOI: 10.1038/s41586-021-04316-2; c) M. Dorn, D. Hunger, C. Förster, R. Naumann, J. van Slageren, K. Heinze, *Chem. Eur. J.* **2023**, 29, e202202898. DOI: 10.1002/chem.202202898; d) K. S. Kumar, D. Serrano, A. M. Nonat, B. Heinrich, L. Karmazin, L. J. Charbonnière, P. Goldner, M. Ruben, *Nat. Commun.* **2021**, *12*, 2152, DOI: 10.1038/s41467-021-22383-x; e) D. W. Laorenza, A. Kairalapova, S. L. Bayliss, T. Goldzak, S. M. Greene, L. R. Weiss, P. Deb, P. J. Mintun, K. A. Collins, D. D. Awschalom, T. C. Berkelbach, D. E. Freedman, *J. Am. Chem. Soc.* **2021**, *143*, 21350–21363; f) S. L. Bayliss, D. W. Laorenza, P. J. Mintun, B. D. Kovos, D. E. Freedman, D. D. Awschalom, *Science* **2020**, *370*, 1309–1312; g) S. Lenz, H. Bamberger, P. P. Hallmen, Y. Thiebes, S. Otto, K. Heinze, J. van Slageren, *Phys. Chem. Chem. Phys.* **2019**, *21*, 6976–6983.
[6] a) C. Wang, F. Reichenauer, W. R. Kitzmann, C. Kerzig, K. Heinze, U. Resch-Genger, *Angew. Chem. Int. Ed.* **2022**, *61*, e202202238; *Angew. Chem.* **2022**, *134*, e202202238; b) P. Bharmoria, H. Bildirir, K. Moth-Poulsen, *Chem. Soc. Rev.* **2020**, *49*, 6529–6554; c) J. Kalmbach, C. Wang, Y. You, C. Förster, H. Schubert, K. Heinze, U. Resch-Genger, M. Seitz, *Angew. Chem.* **2020**, *132*, 18966–18970; *Angew. Chem. Int. Ed.* **2020**, *59*, 18804–18808; d) A. Nonat, S. Bahamyirou, A. Lecointre, F. Przybilla, Y. Mély, C. Platas-Iglesias, F. Camerel, O. Jeannin, L. J. Charbonnière, *J. Am. Chem. Soc.* **2019**, *141*, 1568–1576; e) B. Golesorkhi, H. Nozary, L. Guénée, A. Fürstenberg, C. Piguet, *Angew. Chem. Int. Ed.* **2018**, *57*, 15172–15176; f) N. Souri, P. Tian, C. Platas-Iglesias, K.-L. Wong, A. Nonat, L. J. Charbonnière, *J. Am. Chem. Soc.* **2017**, *139*, 1456–1459; g) A. Nonat, C. F. Chan, C. Platas-Iglesias, Z. Liu, W.-T. Wong, W.-K. Wong, L.-K. Wong, L. J. Charbonnière, T. Liu, *Nat. Commun.* **2016**, *7*. DOI: 10.1038/ncomms11978; h) L. Aboshyan-Sorgho, C. Besnard, P. Pattison, K. R. Kittilstved, A. Aebischer, J.-C. G. Bünzli, A. Hauser, C. Piguet, *Angew. Chem. Int. Ed.* **2011**, *50*, 4108–4112; i) B. Golesorkhi, S. Naseri, L. Guénée, I. Taarit, F. Alves, H. Nozary, C. Piguet, *J. Am. Chem. Soc.* **2010**, *143*, 15326–15334; j) T. N. Singh-Rachford, F. N. Castellano, *Coord. Chem. Rev.* **2010**, *254*, 2560–2573.
[7] a) C. Wang, S. Otto, M. Dorn, K. Heinze, U. Resch-Genger, *Anal. Chem.* **2019**, *91*, 2337–2344; b) S. Otto, J. Harris, K. Heinze, C. Reber, *Angew. Chem.* **2018**, *130*, 11236–11240; *Angew. Chem. Int. Ed.* **2018**, *57*, 11069–11073; c) S. Otto, N. Scholz, T. Behnke, U. Resch-Genger, K. Heinze, *Chem. Eur. J.* **2017**, *23*, 12131–12135; d) M. Schäferling, *Angew. Chem. Int. Ed.* **2012**, *51*, 3532–3554; *Angew. Chem.* **2012**, *124*, 3590–3614; e) I. J. Stich Matthias, S. Nagl, S. O. Wolfbeis, U. Henne, M. Schäferling, *Adv. Funct. Mater.* **2008**, *18*, 1399–1406.
[8] a) W. R. Kitzmann, K. Heinze, *Angew. Chem. Int. Ed.* **2023**, e202213207; b) C. Wegeberg, O. S. Wenger, *Dalton Trans.* **2022**, *51*, 1297–1302; c) W. R. Kitzmann, C. Ramanan, R. Naumann, K. Heinze, *Dalton Trans.* **2022**, *51*, 6519–6525; d) C. Förster, K. Heinze, *Chem. Phys. Rev.* **2022**, *3*, 041302; e) C. Wegeberg, O. S. Wenger, *JACS Au* **2021**, *1*, 1860–1876; f) C. Förster, K. Heinze, *Chem. Soc. Rev.* **2020**, *49*, 1057–1070; g) O. S. Wenger, *J. Am. Chem. Soc.* **2018**, *140*, 13522–13533.
[9] a) R. A. Forman, G. J. Piermarini, J. D. Barnett, S. Block, *Science* **1972**, *176*, 284–285; b) G. J. Piermarini, S. Block, J. D. Barnett, R. A. Forman, *J. Appl. Phys.* **1975**, *46*, 2774–2780; c) R. G. Munro, G. J. Piermarini, S. Block, W. B. Holzapfel, *J. Appl. Phys.* **1985**, *57*, 165–169; d) H. K. Mao, P. M. Bell, J. W. Shaner, D. J. Steinberg, *J. Appl. Phys.* **1978**, *49*, 3276–3283.
[10] a) C. Zhao, H. Li, Y. Wang, J. Jiang, Y. He, *High Pressure Res.* **2017**, *37*, 18–27; b) Q. Jing, Q. Wu, L. Liu, J.-a. Xu, Y. Bi, Y. Liu, H. Chen, S. Liu, Y. Zhang, L. Xiong, Y. Li, J. Liu, *J. Appl. Phys.* **2013**, *113*, 023507; c) F. Datchi, A. Dewaele, P. Loubeyre, R. Letoullec, Y. Le Godec, B. Canny, *High Pressure Res.* **2007**, *27*, 447–463; d) Y. R. Shen, T. Gregorian, W. B. Holzapfel, *High Pressure Res.* **1991**, *7*, 73–75.
[11] J. Liu, R. Tang, Y. Wang, W. Jia, Y. Shang, S. He, *J. Lumin.* **1988**, *40&41*, 419–420.
[12] A. G. Rinzler, J. F. Dolan, L. A. Kappers, D. S. Hamilton, R. H. Bartram, *J. Phys. Chem. Solids* **1993**, *54*, 89–100.
[13] M. Milos, T. Penhouet, P. Pal, A. Hauser, *Inorg. Chem.* **2010**, *49*, 3402–3408.
[14] S. H. Lee, W. L. Waltz, D. R. Demmer, R. T. Walters, *Inorg. Chem.* **1985**, *24*, 1531–1538.
[15] H. Yersin, P. Huber, G. Gietl, D. Trümbach, *Chem. Phys. Lett.* **1992**, *199*, 1–9.
[16] J. W. Kenney III, J. W. Clymire, S. F. Agnew, *J. Am. Chem. Soc.* **1995**, *117*, 1645–1646.
[17] a) S. Otto, M. Grabolle, C. Förster, C. Kreitner, U. Resch-Genger, K. Heinze, *Angew. Chem. Int. Ed.* **2015**, *54*, 11572–11576; *Angew. Chem.* **2015**, *127*, 11735–11739; b) C. Wang, S. Otto, M. Dorn, E. Kreidt, J. Lebon, L. Sršan, P. Di Martino-Fumo, M. Gerhards, U. Resch-Genger, M. Seitz, K. Heinze, *Angew. Chem. Int. Ed.* **2018**, *57*, 1112–1116; *Angew. Chem.* **2018**, *130*, 1125–1130; c) C. Wang, W. R. Kitzmann, F. Weigert, C. Förster, X. Wang, K. Heinze, U. Resch-Genger, *ChemPhotoChem* **2022**, *6*, e202100296; d) L. Stein, C. Wang, C. Förster, U. Resch-Genger, K. Heinze, *Dalton Trans.* **2022**, *51*, 17664–17670.
[18] F. Reichenauer, C. Wang, C. Förster, P. Boden, N. Ugur, R. Báez-Cruz, J. Kalmbach, L. M. Carrella, E. Rentschler, C. Ramanan, G. Niedner-Schatteburg, M. Gerhards, M. Seitz, U. Resch-Genger, K. Heinze, *J. Am. Chem. Soc.* **2021**, *143*, 11843–11855.
[19] S. Treiling, C. Wang, C. Förster, F. Reichenauer, J. Kalmbach, P. Boden, J. P. Harris, L. Carrella, E. Rentschler, U. Resch-Genger, C. Reber, M. Seitz, M. Gerhards, K. Heinze, *Angew. Chem.* **2019**, *131*, 18243–18253; *Angew. Chem. Int. Ed.* **2019**, *58*, 18075–18085.
[20] S. Otto, C. Förster, C. Wang, U. Resch-Genger, K. Heinze, *Chem. Eur. J.* **2018**, *24*, 12555–12563.
[21] W. R. Kitzmann, J. Moll, K. Heinze, *Photochem. Photobiol. Sci.* **2022**, *21*, 1309–1331.
[22] a) M. Dorn, J. Kalmbach, P. Boden, A. Kruse, C. Dab, C. Reber, G. Niedner-Schatteburg, S. Lochbrunner, M. Gerhards, M. Seitz, K. Heinze, *Chem. Sci.* **2021**, *12*, 10780–10790; b) M. Dorn, J. Kalmbach, P. Boden, A. Päpcke, S. Gómez, C. Förster, F. Kuczelinis, L. M. Carrella, L. Büldt, N. Bings, E. Rentschler, S. Lochbrunner, L. González, M. Gerhards, M. Seitz, K. Heinze, *J. Am. Chem. Soc.* **2020**, *142*, 7947–7955.
[23] A. P. Jephcoat, R. J. Hemley, H. K. Mao, *Physica B + C* **1988**, *150*, 115–121.
[24] M. Atanasov, D. Ganyushin, K. Sivalingam, F. Neese, *Struct. Bonding (Berlin)* **2011**, *143*, 149–220.
[25] S. K. Singh, J. Eng, M. Atanasov, N. Neese, *Coord. Chem. Rev.* **2017**, *344*, 2–25.
[26] L. Lang, M. Atanasov, F. Neese, *J. Phys. Chem. A* **2020**, *124*, 1025–1037.
[27] CP2k, General program to perform molecular dynamics simulations, CP2k developers group under the terms of the GNU General Public License. CP2k is freely available from www.cp2k.org.
[28] J. VandeVondele, J. Hutter, *J. Chem. Phys.* **2007**, *127*, 114105.
[29] S. Goedecker, M. Teter, J. Hutter, *Phys. Rev. B* **1996**, *54*, 1703–1710.
[30] C. Hartwigsen, S. Goedecker, J. Hutter, *Phys. Rev. B* **1998**, *58*, 3641–3662.
[31] M. Krack, *Theor. Chem. Acc.* **2005**, *114*, 145–152.
[32] J. P. Perdew, K. Burke, M. Ernzerhof, *Phys. Rev. Lett.* **1996**, *77*, 3865–3868.
[33] S. Grimme, S. Ehrlich, L. Goerigk, *J. Comput. Chem.* **2011**, *32*, 1456–1465.
[34] J. Schmidt, J. VandeVondele, I.-F. W. Kuo, D. Sebastiani, J. I. Siepmann, J. Hutter, C. J. Mundy, *J. Phys. Chem. B* **2009**, *113*, 11959–11964.
[35] F. Neese, *WIREs Comput. Mol. Sci.* **2012**, *2*, 73–78.
[36] F. Neese, *WIREs Comput. Mol. Sci.* **2022**, *12*, e1606.
[37] C. Lee, W. Yang, R. G. Parr, *Phys. Rev. B* **1988**, *37*, 785–789.
[38] B. Miehlich, A. Savin, H. Stoll, H. Preuss, *Chem. Phys. Lett.* **1989**, *157*, 200–206.
[39] A. D. Becke, *J. Chem. Phys.* **1993**, *98*, 5648–5652.
[40] F. Weigend, R. Ahlrichs, *Phys. Chem. Chem. Phys.* **2005**, *7*, 3297–3305.
[41] F. Weigend, *J. Comput. Chem.* **2008**, *29*, 167–175.
[42] F. Neese, F. Wennmohs, A. Hansen, U. Becker, *Chem. Phys.* **2009**, *356*, 98–109.
[43] R. Izsák, F. Neese, *J. Chem. Phys.* **2011**, *135*, 144105.
[44] F. Weigend, M. Kattanek, R. Ahlrichs, *J. Chem. Phys.* **2009**, *130*, 164106.
[45] C. Angeli, R. Cimiraglia, S. Evangelisti, T. Leininger, J. P. Malrieu, *J. Chem. Phys.* **2001**, *114*, 10252–10264.

[46] C. Angeli, R. Cimiraglia, J. P. Malrieu, *J. Chem. Phys.* **2002**, *117*, 9138–9153.
[47] D. A. Pantazis, F. Neese, *J. Chem. Theory Comput.* **2009**, *5*, 2229–2238.
[48] D. A. Pantazis, X.-Y. Chen, C. R. Landis, F. Neese, *J. Chem. Theory Comput.* **2008**, *4*, 908–919.
[49] D. A. Pantazis, F. Neese, *Theor. Chem. Acc.* **2012**, *131*, 1292.
[50] D. A. Pantazis, F. Neese, *J. Chem. Theory Comput.* **2011**, *7*, 677–684.
[51] C. van Wüllen, *J. Chem. Phys.* **1998**, *109*, 392–399.
[52] E. van Lenthe, E. J. Baerends, J. G. Snijders, *J. Chem. Phys.* **1993**, *99*, 4597–4610.
[53] S. Miertus, E. Scrocco, J. Tomasi, *Chem. Phys.* **1981**, *55*, 117–129.
[54] V. Barone, M. Cossi, *J. Phys. Chem. A* **1998**, *102*, 1995–2001.

Manuscript received: March 3, 2023
Revised manuscript received: March 28, 2023
Accepted manuscript online: March 29, 2023
Version of record online: ■■, ■■